Bulletin of the Seismological Society of America, Vol. 93, No. 3, pp. 1370–1380, June 2003

What Can Superconducting Gravimeters Contribute to Normal-Mode Seismology?

by R. Widmer-Schnidrig

Abstract The seismic free oscillations of the Earth can be observed in the frequency band from 0.3 to 20 mHz, and estimates of their frequencies constitute the principal constraints for spherically symmetric Earth models such as the Preliminary Reference Earth Model (PREM). While the bulk of the mode observations rely on recordings of the spring gravimeters deployed in the International Deployment of Accelerometers (IDA) network and more recently on the Streckiesen STS-1 seismometers deployed in the global seismic network (GSN), we show here that the most recent generation of superconducting gravimeters (SGs) can achieve lower noise levels than either one of the aforementioned sensors at frequencies lower than ~0.8 mHz.

While the splitting of modes above 1 mHz is largely due to structural heterogeneities in *P*- and *S*-wave velocities, the modes below 1 mHz are unique for two reasons: (1) the destabilizing effect of self-gravitation leads to a high sensitivity to density heterogeneities and (2) the vicinity of these modes to the frequency of the Earth's rotation leads to pronounced Zeeman splitting, which in turn depends on spherically averaged density structure. Thus it is argued that SGs can make a significant contribution to the illumination of long-wavelength density heterogeneities in the Earth's mantle.

At frequencies above 1 mHz, current SGs exhibit higher noise levels than the quietest seismometers deployed in the GSN. Furthermore we show that above 3 mHz, even the Streckeisen STS-2 seismometers compare favorably against the SGs if the former are installed with elaborate shielding from environmental effects.

Introduction

Superconducting gravimeters (SGs) (e.g., Warburton and Brinton, 1995; Goodkind, 1999) currently deployed in the sparse Global Geodynamics Project (GGP) network (Crossley *et al.*, 1999) hold the promise to achieve lower instrumental noise levels over sensors currently deployed in the global seismographic network (GSN) and used in studies of the Earth's free oscillations. This position article attempts to review the current situation in observational normal-mode seismology both from the point of view of instrumental challenges and challenges related to the illumination of the Earth's large-scale structure. Particular attention is given to 1D and 3D density structure and how this structure is encoded in the observable normal-mode spectra. The reason for concentration on density structure is that the frequency band where SGs compare most favorably with seismic sensors coincides with the band where the modes have increased sensitivity to laterally heterogeneous as well as 1D density structure through the mechanism of self-gravitation. Since our ability to learn about Earth structure is always a question of signal-to-noise ratio (SNR) in our data, we have organized the article into a discussion of instrumental and environmental noise followed by a discussion of normal-mode signals. The article concludes with an assessment of where SGs can make a difference in our quest to learn about deep Earth structure.

Vertical Seismic Noise

Global Noise Models

The level of background seismic noise limits our ability to detect small seismic signals that have propagated through the Earth and that carry information about both their source and the structure of the medium through which they propagated. Comprehensive studies of typical and of minimum noise levels have been carried out to asses station performance and to help in site selection and in negotiations of nuclear-test-ban treaties (e.g., Agnew and Berger, 1978; Peterson, 1993; Astiz and Creager, 1995). Figure 1 shows the new low-noise model (NLNM) of Peterson (1993), which is

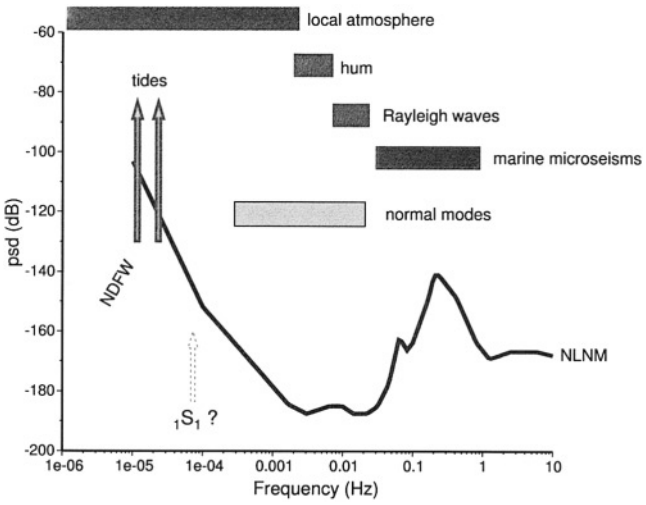

Figure 1. Dominant sources of seismic noise on vertical component sensors (i.e., gravimeters and vertical seismometers) together with the new low-noise model (NLNM) of Peterson (1993). The NLNM is given in power spectral densities in units of decibels relative to 1 $(m/sec^2)^2/Hz$. While there exist of course many more sources of seismic noise related to poor installations, insufficient shielding of sensors, noisy sites, and so on, the sources indicated here are what limit the detection of small signals given optimal installation conditions and optimally performing sensors. Also indicated is the normal-mode band, the principal tidal bands, the nearly diurnal free wobble (NDFW), and the suspected location of the Slichter mode, $_1S_1$.

the lower envelope of noise levels found at GSN stations. A number of different sensors are deployed at the GSN stations; however, below 30 mHz the NLNM is largely defined by recordings from Streckeisen STS-1 seismometer.

Many of the large features of the NLNM are well understood. At frequencies below 2 mHz the Newtonian attraction of moving air masses in the local atmosphere above the seismic sensor is the principal source of noise (e.g., Warburton and Goodkind, 1977; Zürn and Widmer, 1995).

In the band 2–7 mHz the NLNM exhibits a slight minimum near 3 mHz but is otherwise relatively flat. Recent studies of the noise floor in this band with high-frequency resolution have revealed that the noise floor contains a well-defined structure consisting of ~50 regularly spaced peaks whose frequencies coincide with the fundamental spheroidal modes, $_0S_\ell$ (e.g., Suda *et al.*, 1998). This structure in the noise floor is termed "background free oscillations" or simply "hum." Since free oscillations are a global phenomenon, the hum constitutes a lower bound for observable signals at any site on the Earth's surface. The hum amplitude has also been found to be very stable in time, with only a small semi-annual harmonic component. In the band 7–30 mHz the NLNM exhibits a local maximum near 10 mHz.

The cause for the generally level noise floor between 2 and 30 mHz is still not understood. However Nishida *et al.* (2002) were able to demonstrate that in the band adjacent to the hum, (7–30 mHz) the background noise consists of globe-circling Rayleigh waves much like the hum (Ekström, 2001). The physical process involved in the hum excitation is still a matter of debate, with turbulence in the atmosphere and/or hydrosphere being the favored candidates.

One problem with identifying the source is the small size of the signal: to drive one of the spheroidal multiplets at the observed root mean square amplitudes (~1 nGal or 5×10^{-10} m/sec at 300 sec period, a typical quality factor for fundamental spheroidal modes of $Q \sim 300$, and an effective mass of the upper mantle of $m \sim 10^{24}$ kg) requires approximately 10 W of power! Another more serious problem is that the hum signal is very close to the detection limit of current sensors (discussed later).

In the band from 30 mHz to 1 Hz background noise levels are dominated by the marine microseism with a peak around 0.14 Hz. The cause of the microseisms are the swell- and surf-induced pressure fluctuations at the bottom of the water column, which excite seismic waves in the solid Earth. It is very fortunate for the study of normal modes that the normal-mode band (0.3–20 mHz; Fig. 1) and the band of microseism (30 mHz–1 Hz) do not overlap, considering that noise levels in the microseism band are often 60 dB higher than in the band of the hum.

Noise Levels at the Black Forest Observatory

The Black Forest Observatory (BFO) is particularly suited for noise studies for two reasons: (1) noise levels at BFO have been repeatedly shown to be among the lowest of the GSN (e.g., Zürn *et al.*, 2000) and (2) these low noise levels have been achieved simultaneously with up to four different sensors (Richter *et al.*, 1995). Thus one can attempt to answer the following question: to what extent is the NLNM defined by the instrumental noise of the sensors or by seismic noise? While this distinction is impossible to make with a single sensor, it is also dangerous to conclude from global studies such as Peterson (1993) that the universality of the NLNM is a feature of the Earth's seismic background. Considering that the NLNM below 20 mHz relies primarily on data from STS-1 seismometers, it is conceivable that the NLNM reflects (at least in some bands) the instrumental noise of the STS-1.

With multiple colocated sensors it is in principle possible to separate sensor noise from seismic noise. Seismic noise should be common to all sensors, while sensor noise should be uncorrelated between the different sensors. To get a robust and representative estimate of seismic noise at BFO, we have selected data from the vertical component STS-1 seismometer (VHZ) recorded on a 24-bit channel of the IDA Mk7 data logger, the TIDE channel of the LaCoste–Romberg ET-19 gravimeter (UGZ) recorded on a 16-bit auxiliary channel of the IDA Mk7 logger, and the long-period channel (LHZ) of the STS-2 seismometer of the German Regional Seismic Network (GRSN) recorded with 24 bits on a Quanterra Q680 data logger. Continuous data from a 3-

year window (1996:206–1999:179) was chopped into 24-hr-long, overlapping segments with start times at midnight and at noon. Segments were only retained if data from all three sensors was complete. Power spectral densities (PSDs) were computed and integrated between 3 and 5 mHz to give a single number representative of the noise level in the normal mode band. Based on a histogram of these noise levels a selection of 895 quiet windows was made, for which all three sensors simultaneously meet our noise criterion. Thus 60% of the windows were rejected.

Figure 2 (top) shows the average PSDs for the three sensors compared with the NLNM of Peterson (1993). PSDs are computed following Press *et al.* (1987): we have removed mean and linear trend prior to fast Fourier transforming the signals and applied a Hanning taper in the time domain to suppress spectral leakage. Furthermore our PSDs are single sided and normalized such that Parzeval's theorem is met: that is, the variance of the signal in the time domain is equal to the PSD integrated from 0 to the Nyquist frequency.

While the PSDs of all sensors are higher than the NLNM, one should keep in mind that the NLNM represents the lower envelope of noise levels encountered on sensors of the GSN, while the PSDs of the sensors from BFO represent average noise levels. In a separate study we have used order statistics to inspect the same ensemble of noise spectra and found that the median over the entire band is slightly but consistently lower than the arithmetic mean and that for all three sensors the first quartile is $\simeq$4 dB lower than the median. The first quartile is comparable with the data selection rules used for the seismic noise magnitude (Banka and Crossley, 1999), which is used in many noise studies of SGs. Noise levels 4 dB lower than given for the STS-1 in Figure 2 are indistinguishable from the NLNM, which confirms our assertion that BFO belongs to the quietest stations of the GSN.

At frequencies below 2 mHz the PSD of the STS-1 and the ET-19 sensors are practically identical. However if we apply the barometric pressure correction, which consists in subtracting the best-fitting, scaled version of the locally recorded atmospheric pressure from the seismic record (Zürn and Widmer, 1995), PSD levels drop by different amounts. While there are many physical mechanisms by which fluctuations in atmospheric pressure can influence seismic recordings, inspection of the histograms in Figure 3 shows that the regression coefficients scatter around a value consistent with the theoretical predictions for the combined effects of the gravitational attraction of the atmosphere and the free-air gravity effect from the downward displacement of the sensors by atmospheric loading (e.g., Zürn and Widmer, 1995). Thus the uncorrected PSDs are governed by gravity signal from the atmospheric pressure fluctuations.

At 0.3 mHz the pressure correction reduces PSD levels by $\sim$2 dB for the STS-1 but by as much as 7 dB for ET-19. Thus it becomes clear that self-noise of the STS-1 in this band is only slightly below the signal PSD. The low efficiency of the pressure correction for the STS-1 could be due to a noisy integral feedback. To check this hypothesis the

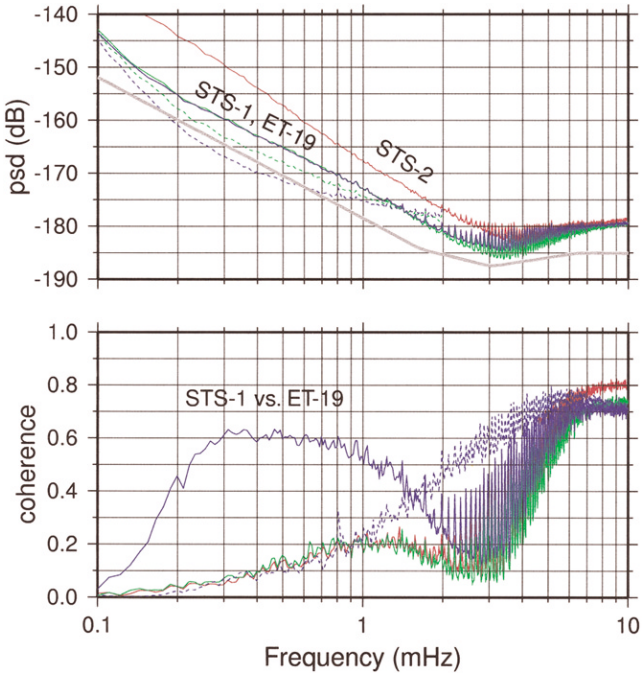

Figure 2. Comparison of the three vertical component seismic sensors installed at BFO: LaCoste–Romberg gravimeter ET-19 and Streckeisen STS-1 and STS-2 seismometers. Shown are the mean noise levels averaged over the 895 selected windows (upper panel). The dashed curves are the pressure-corrected STS-1 (green) and ET-19 (blue) noise levels (Zürn and Widmer, 1995). For the STS-2 (red) the pressure correction is ineffective. The NLNM (gray) is shown for reference. The lower panel shows average pairwise coherencies: STS-2 versus STS-1 (red), STS-2 versus ET-19 (green), and STS-1 versus ET-19 (blue). The coherencies between the STS-2 and either STS-1 or ET-19 are low below $\sim$5 mHz due to the increased self-noise of the STS-2. In the band 2–4 mHz the coherency between STS-1 and ET-19 is also very low, which shows that in this band the self-noise levels of these two sensors are comparable to the level of the coherent signal of the hum. The dashed blue curve in the lower panel is the coherency between the pressure-corrected spectra of ET-19 and STS-1. Its low value for frequencies less than 1 mHz shows that at least one of the sensors (the STS-1) is limited by self-noise after the pressure correction. Since the pressure correction is only marginally efficient for the STS-1 and since noise levels of STS-1 (solid green) and ET-19 (solid blue) without pressure correction are practically identical, we conclude that the NLNM in this band is defined by the barometric effect. The increase of the pressure-corrected coherency above 1 mHz is an artifact of the pressure correction, which only reduces noise levels below 1.5 mHz. Finally, we note the small peak in the pressure-corrected coherency at 0.81 mHz: the frequency of ${}_0S_0$.

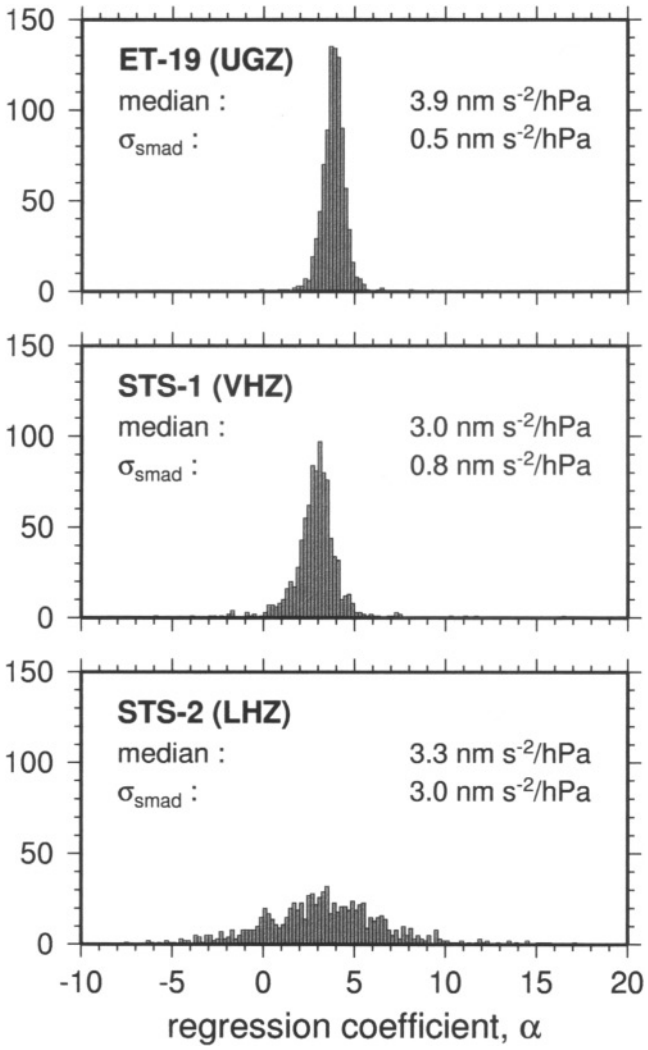

Figure 3. Histograms of 895 regression coefficients for the pressure correction. The regression was carried out in the band 0.1–0.5 mHz. Note the large dispersion for the STS-2. σ_{SMAD} is the scaled median absolute deviation of the median, a statistically robust measure of dispersion equivalent to the standard deviation. The theoretically expected value for the regression coefficient is 3–4 N m sec^{-2}/hPa depending on the atmospheric model and the elastic moduli of the ground around the station.

electronics of the STS-1 at BFO were modified, but this modification did not lead to any improvement (E. Wielandt and W. Zürn, personal comm., 1999).

The pairwise coherencies are given in the lower panel of Figure 2. The low coherencies for the hum show that the hum is at or slightly below the instrument noise levels. This is also the reason that the hum can only be detected after averaging over enough data windows. Figure 4 zooms in on the hum part of Figure 2. In the band of the hum the STS-1 seems to be the sensor with the lowest self-noise, followed by the ET-19 and STS-2. The comblike structure of the spectra is typical for the hum. Note the slight increase of the hum near 3.7 mHz in the PSD of all three sensors. This amplification of the hum was noted by Nishida *et al.* (2000) and constitutes the most direct observational evidence for atmospheric excitation of the hum. Note that at 4 mHz the STS-2 is only 3 dB noisier than the STS-1, while this difference increases to 10 dB at the frequency of ${}_0S_2$ or 0.3 mHz.

The pressure correction leads to no reduction in the noise level for the STS-2 seismometer, implying that this sensor is limited by self-noise at frequencies lower than the band of the hum (~2 mHz).

Noise Levels of SGs

Since we do not operate a permanently installed SG meter at BFO, we refer to published comparisons of SG noise levels and our permanent sensors: Richter *et al.* (1995) have compared data from the seismometers and the LaCoste–Romberg gravimeter with a temporarily installed, portable SG (SG102), while Banka and Crossley (1999) and more recently Van Camp (1999) compared SGs contributing to the GGP network with our sensors.

For frequencies above 1.5 mHz these studies find that the STS-1 and ET-19 at BFO are less noisy than the SGs. This finding has also been confirmed in studies of the hum at Canberra (Australia), where an STS-1 and an SG are colocated (Nawa *et al.*, 2000). In the hum band average noise levels for the STS-1 are ~7 dB lower than for the best SGs while ET-19 is only 4 dB lower. (These numbers were obtained by converting the noise-magnitude estimates of Van Camp [1999] into equivalent PSD values.) This difference in noise levels is also consistent with the observation that the PSD levels of the best SGs intersect, after pressure correction, the NLNM at a frequency of ~1 mHz and are flat above 1 mHz.

For frequencies below 1.0 mHz, where the barometric pressure correction is efficient for gravimeters, the best SGs are less noisy than the STS-1 seismometer. While SGs could still not compete with the ET-19 gravimeter in this band back in 1994 (Richter *et al.*, 1995), recent improvements in SGs has changed this picture (Zürn *et al.*, 2000). In this article data from the Balleny Islands event (1998) recorded by the Incorporated Research Institutions for Seismology (IRIS), GEOSCOPE, and GGP networks was systematically scanned for signals of Coriolis coupled modes below 1 mHz, and the highest SNR was found in the spectra of SGs and ET-19. The most recent occasion for the observation of the gravest normal modes was the Peru event with moment magnitude M_W 8.4 on 23 June 2001, and the spectrum of the SG near Strasbourg (J9) is shown together with the spectrum of the 1977 Sumbawa event (M_W 8.3) recorded in Brasilia with the IDA gravimeter at Brasilia (BDF) in Figure 5. The spectrum from BDF was up until now the spectrum with the highest SNR for the football mode, ${}_0S_2$. For the Peru event this mode was detected with a similar SNR in spectra of SGs located in Vienna (Austria), Metsähovi (Finland), Moxa (Germany), and Southerland (South Africa), and their high SNR for ${}_0S_2$

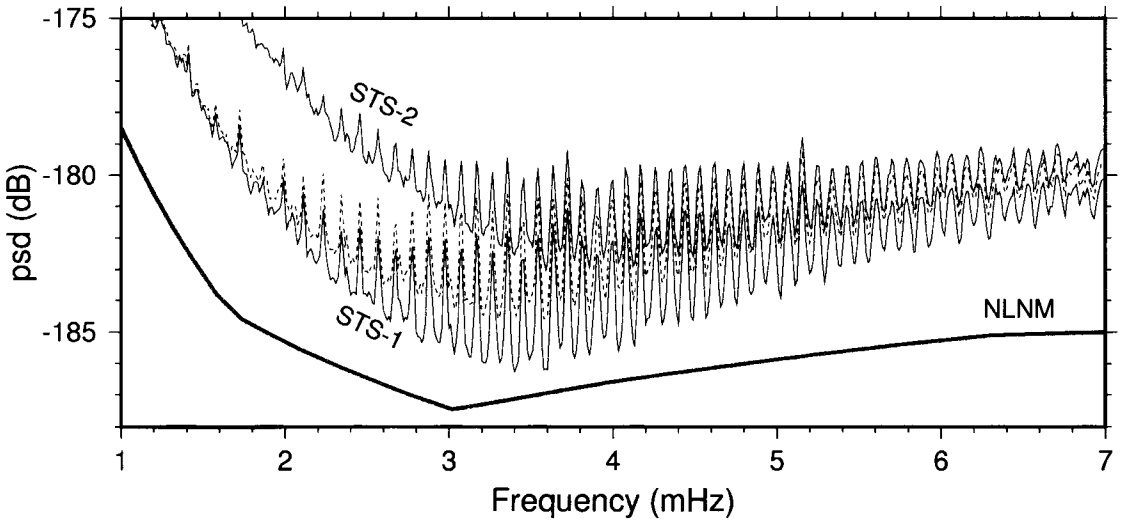

Figure 4. Blowup of upper panel of Figure 2. The lowest curve is from the STS-1, followed by the ET-19 (dashed) and the STS-2.

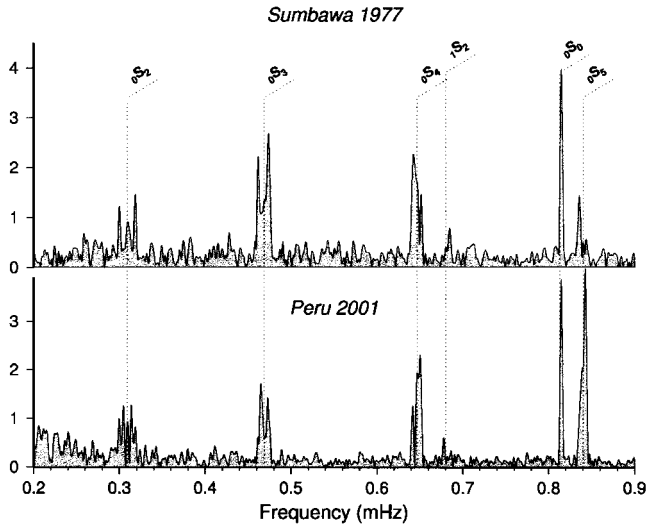

Figure 5. Comparison of two linear amplitude spectra from events separated by 24 years. The upper spectrum is for the 1977 M_w 8.3 Sumbawa event recorded with the LaCoste–Romberg gravimeter at BDF (Brasilia, Brazil) connected to a 12-bit analog to digital converter. The lower spectrum is for the 2001 M_w 8.4 Peru event recorded by the SG at J9 (Strasbourg, France). Record length is 150 hr for Sumbawa and 167 hr for the Peru event. Note that only the spectrum from the Peru event is pressure corrected.

could not be matched with either ET-19 or any of the STS-1s of the GSN. In other words the most recent version of SGs is now competitive with the best spring gravimeters as far up in frequency as 1.5 mHz, and below ~0.6 mHz SGs are, after pressure correction, clearly superior to either spring gravimeters or STS-1 seismometers.

Above 3 mHz, however, it seems that the best SGs cannot compete with the STS-2 at BFO. To corroborate the low noise level of the STS-2 at BFO, we show a spectrogram of 2 years of continuous data (Fig. 6) together with a robust estimate of the noise levels of that sensor. While one might suspect that this low noise level of the STS-2 is due to the very elaborate shielding of the sensors at BFO, it should be noted that we detected the hum at 7 out of 14 STS-2 equipped stations of the GRSN.

The low noise level of the STS-2 above 3 mHz, while higher than STS-1 or ET-19, is of some practical relevance, since manufacturing of both LaCoste–Romberg ET meters as well as STS-1 seismometers has been discontinued, making the STS-2 the quietest commercially available sensor in this band. Of course we are aware that there exist other commercially available broadband seismometers. However our inspection of data from the Geotech KS-54000 borehole seismometer deployed in the GSN has not revealed any signs of the hum. Furthermore we are unaware of any published hum detections for that sensor. The same is true for broadband seismometers manufactured by Guralp.

Normal Modes in Seismic Data

Before the Earth's normal modes can be detected as discrete peaks in spectra of earthquake recordings, a number of criteria must be met: The earthquake source must exceed a minimum moment magnitude of M_w ~6.5. Since the modes can be viewed as the interference of waves traveling in opposite directions around the globe, the minimum time series length to Fourier analyze must be larger than the 3 hr needed for one orbit. In order to maximize frequency resolution one has to increase the record length. In practice one faces a trade-off between frequency resolution and available signal. Increasing the time series length improves frequency resolution. However, since the modes get attenuated, there comes a point after which one adds only noise if one keeps

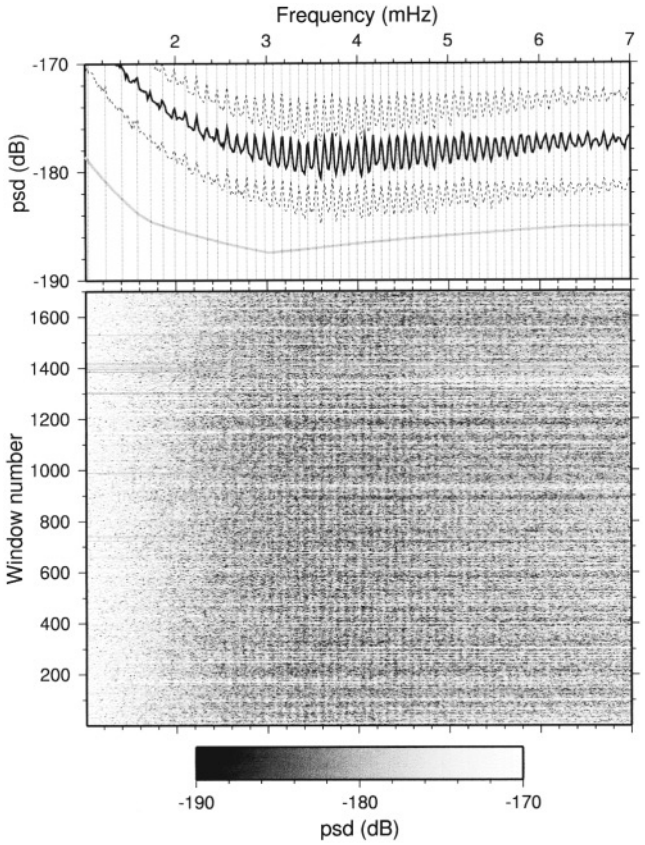

Figure 6. Time-frequency plot covering 2 years of data from the STS-2 seismometer of the German Regional Seismic Network (GRSN) at BFO. The range of the grayscale is chosen to emphasize structure in the noise during seismically quiet times. The upper panel shows median PSD levels (black) together with the first and third quartile (dashed). The NLNM (gray) is shown for reference. The vertical dashed lines indicate the predicted frequencies of the fundamental spheroidal modes ${}_0S_\ell$ and coincide with light-gray vertical bands in the lower panel.

increasing time series length. A good compromise between frequency resolution and SNR can be obtained for a record length of Q cycles (Dahlen, 1979).

Earth structure is encoded in two ways in normal-mode spectra: spherically averaged Earth structure can be inferred from multiplet degenerate frequencies, while aspherical structure information can be gleaned either from the splitting of individual multiplets or from the coupling between multiplets. Since the Earth is very nearly spherical, one can understand that splitting and coupling of modes are subtle effects in the observed spectra, and hence it should not surprise that deviations from sphericity are much less well constrained than spherically averaged Earth structure.

Encoding of 1D Earth Structure in Mode Spectra

Estimates of multiplet degenerate frequencies can be obtained from a number of different techniques; a first set of techniques treats the effect of aspherical structure as a source of random errors, and by analyzing spectra from enough earthquakes with a well-distributed set of stations, one hopes that it will average out (e.g., multiplet stripping and stacking [Gilbert and Dziewonski, 1975]).

A second set of techniques strives to extract constraints about 3D structure, and as an aside one always also gets a degenerate frequency estimate that is largely free from bias due to effects from 3D structure. These techniques are histogram analysis of single-record peak frequency measurements (e.g., Smith and Masters, 1989), iterative spectral fitting (e.g., Ritzwoller *et al.*, 1988; Resovsky and Ritzwoller, 1998) and the autoregressive method (Masters *et al.*, 2000). While these techniques provide the most precise degenerate frequency estimates, they can only by applied to two small subsets of modes. These are on the one hand the fundamental toroidal and spheroidal modes and on the other hand the high-Q, low-ℓ, spheroidal overtones. All overtones with $\ell \geq 10$ could, until recently, only be analyzed with multiplet stripping. With the increasing number of high-quality recordings of large earthquakes during the last decade, a regionalization of the multiplet stripping technique became feasible for many high-ℓ overtones (Widmer-Schnidrig, 2002), which provided both improved degenerate frequency estimates as well as the first, crude 3D constraints from these modes. Figure 7 summarizes where in the ω-ℓ plane the different techniques mentioned have been applied.

The datasets used for the analysis of high-Q, low-ℓ modes consist typically only of the $\sim$50 records for each of the $\sim$10 largest events. For the high-ℓ modes, however, much larger datasets are used: the regionalized multiplet stripping experiments were only possible because a dataset of 12,000 individual traces (6000 vertical and 6000 horizontal component recordings) was available.

Table 1 gives the distribution of errors for a recently compiled dataset of multiplet degenerate frequencies (see Widmer-Schnidrig [2002] and the Reference Earth Model web site, http://mahi.ucsd.edu/Gabi/rem.html). None of the frequencies in this dataset have been derived from SG recordings; in fact we are unaware of any multiplet degenerate frequency measurements derived from SG data and published in the literature.

Applying Backus–Gilbert resolution analysis to this dataset, we find that all five elastic parameters of a transversely isotropic medium plus the density can be estimated with high radial resolution and very little trade-off between the parameters. Figure 8 depicts the density averaging kernels obtained from the aforementioned dataset. The target uncertainty was set to 0.1%, and the bell-shaped kernels show over which depth range the model has to be integrated in order to achieve this error level. The target depth was varied from frame to frame and shows how resolution degrades with depth.

In Figure 8 the trade-off with other parameters becomes only noticeable in the core where the averaging kernels for the elastic parameters (drawn in black) are nonvanishing.

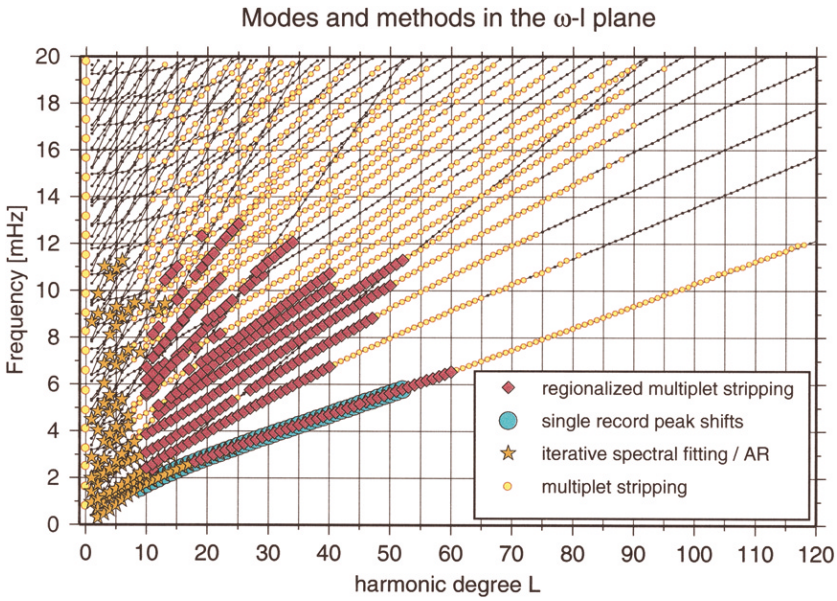

Figure 7. Spheroidal-mode dispersion diagram for model PREM. The symbols used for the different modes indicates the analysis technique with which the mode was observed: regionalized multiplet stripping (Widmer-Schnidrig, 2002), single record peak shifts (e.g., Smith and Masters, 1989), iterative spectral fitting (e.g., Ritzwoller *et al.*, 1988), autoregressive method (AR) (Masters *et al.*, 2000), and multiplet stripping (Masters and Widmer, 1995).

Table 1
Distribution of Relative Errors in Multiplet Degenerate Frequency Dataset used for the Construction of New 1D Earth Models

σ	${}_nS_\ell$	${}_nT_\ell$	${}_nS_0$
1×10^{-5} to 3×10^{-5}	0	0	1
3×10^{-5} to 1×10^{-4}	56	2	13
1×10^{-4} to 3×10^{-4}	279	48	10
3×10^{-4} to 1×10^{-3}	712	198	0
1×10^{-3} to 3×10^{-3}	325	39	0

At this point no SG data has as yet been included in the estimation of any of the frequencies listed here. σ is the range in relative errors; ${}_nS_0$ are the radial modes.

This means that leakage from elastic parameters biases the density estimates.

Since the density, ρ, is the geodynamically most interesting parameter, any further improvement in the radial density profile should be welcome. The need to improve 1D density models is emphasized by noting that for the discussion of the stability of stratification, the relevant parameter is not the density, $\rho(r)$, but the less well resolved radial derivative, $d\rho/dr$.

Here we recall two possible avenues to improve on 1D density models: the observation of Zeeman splitting of individual multiplets and Coriolis coupling between spheroidal and toroidal multiplets. Zeeman splitting and Coriolis coupling are small signals and need to be observed with high precision before any new inference about Earth structure can be drawn from them. The reward, however, would be significant, since these observables constitute linear constraints on the 1D density profile much like the Earth's mass and moment of inertia. Thus their interpretation is not subject to any trade-off with elastic parameters.

Splitting Due to Rotation: Zeeman Splitting

The rotation of the Earth completely removes the degeneracy of a spheroidal multiplet, ${}_nS_\ell$. The frequencies of the $2\ell + 1$ singlets become

$$\omega_m = \bar{\omega} + \delta\omega_m = \bar{\omega}(1 + mb) \quad \text{for} \quad -\ell \le m \le \ell, \tag{1}$$

with Ω the rotation rate of the Earth, $\bar{\omega}$ the multiplet degenerate frequency, and $-\ell \le m \le \ell$ the azimuthal order of the singlet and b the Zeeman splitting parameter. If the singlet frequencies of the $2\ell + 1$ singlets can be observed (such as for ${}_0S_2$ in Fig. 5), one can estimate b based on equation (1). For the kth multiplet b_k is related to the distribution of density with depth through the integral relation (Backus and Gilbert, 1961)

$$\frac{\bar{\omega}}{\Omega} b_k = \frac{\int \rho[2U_k V_k + V_k^2]r^2 dr}{\int \rho[U_k^2 + \ell(\ell+1)V_k^2]r^2 dr}, \tag{2}$$

where $U_k(r)$ and $V_k(r)$ are the usual scalar radial eigenfunction of the kth spheroidal multiplet. The denominator corresponds to the kinetic energy of the mode and is used to normalize the eigenfunctions to unity. One is thus left with a linear relation between the b_k's and the density.

In a pilot study based on the singlet stripping technique (Widmer *et al.*, 1992a), I estimated rotational splitting parameters (Table 2) for all spheroidal multiplets for which rotational splitting is expected to play a dominant role. While the errors in the splitting parameters are considerably larger than in the degenerate frequency dataset (see Table 1), these parameters have the advantage of depending on density only, and hence their interpretation is not subject to any ambiguity with the anisotropic elastic parameters.

Estimation of rotational splitting parameters is some-

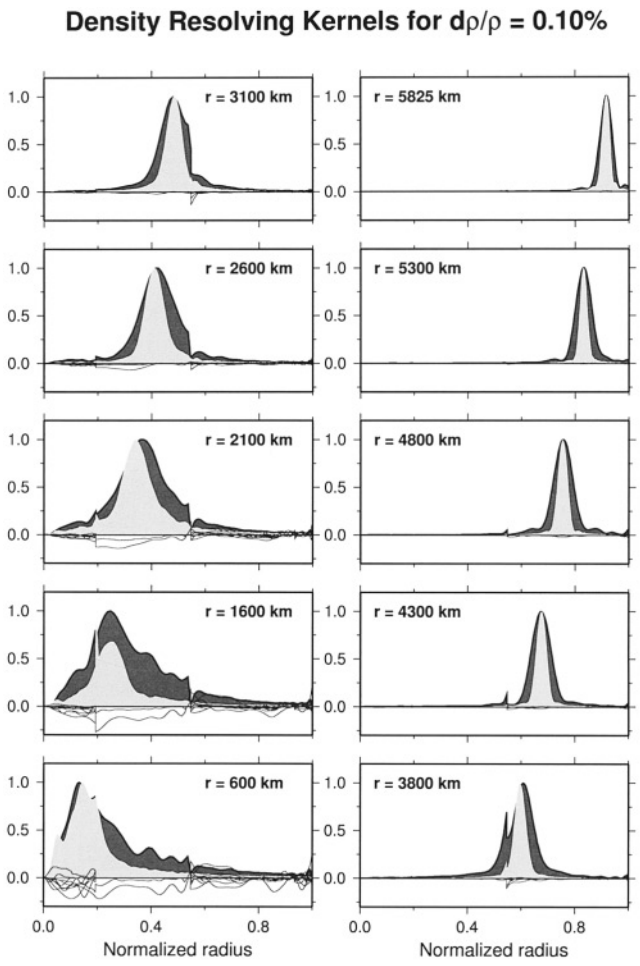

Figure 8. Backus-Gilbert type resolution analysis for the radial distribution of density. The narrower (light gray) averaging kernels include the new degenerate frequency estimates made possible by the sequence of large events in 1994. The wider (dark) averaging kernels are solely based on the degenerate frequency dataset compiled in Masters and Widmer (1995), which was derived from earthquake recordings prior to 1994. The width of the bell-shaped curve is a measure of the ability of the data to concentrate information regarding a particular parameter (here density) and a given relative error (0.1%). The data of the events in 1994 have significantly improved our ability to resolve 1D density structure.

thing that data from SGs should be particularly suited for. Rotational splitting is largest for low-frequency multiplets because of their vicinity to the rotation frequency, Ω. The band below 2 mHz is also the band where the barometric pressure correction (Zürn and Widmer, 1995) is effective and where the best SGs have outperformed seismometers.

Coupling Due to Rotation: Coriolis Coupling

Coriolis coupling between fundamental spheroidal and fundamental toroidal modes has been well observed between 1 and 3.5 mHz (Masters *et al.*, 1983) and more recently also in the band below 1 mHz (Zürn *et al.*, 2000). In fact, apart from the spectra of the strain meter array at BFO (Widmer *et al.*, 1992b), the SGs have contributed some of the best detections of the fundamental toroidal mode, ${}_0T_2$, which only shows up in vertical component recordings through Coriolis coupling with nearby spheroidal multiplets.

Here we would only like to repeat what was already pointed out by Zürn *et al.* (2000), namely that Coriolis coupling provides linear constraints on the density profile, very similar to Zeeman splitting. The difficulty with interpreting observations of Coriolis coupling is that one needs a spherically symmetric reference model that accurately predicts the frequency separation of the coupling partners. While neither the Preliminary Reference Earth Model (PREM) nor 1066A have met this criterion, the next generation of 1D reference models may well fill in this need.

Table 2
Zeeman Splitting Parameter of Selected Low-Frequency Spheroidal Modes

Mode	f_{1066A} (mHz)	b_{obs} ($\times 10^{-3}$)	r (%)	b_{1066A}	b_{PREM}
${}_0S_3$	0.468	4.67 ± 0.16	3.4	4.6216	4.6266
${}_0S_4$	0.647	1.80 ± 0.047	2.6	1.8342	1.8373
${}_0S_5$	0.840	0.83 ± 0.028	3.4	0.8416	0.8442
${}_0S_6$	1.037	0.43 ± 0.015	3.5	0.4070	0.4097
${}_1S_3$	0.940	2.728 ± 0.053	1.9	2.6321	2.6388
${}_1S_4$	1.174	2.007 ± 0.048	2.4	1.9478	1.9494
${}_1S_5$	1.371	1.489 ± 0.067	4.5	1.4363	1.4362
${}_1S_8$	1.798	0.458 ± 0.020	4.4	0.4271	0.4284
${}_2S_4$	1.377	0.087 ± 0.107	122.0	0.2809	0.2840
${}_2S_8$	2.049	0.344 ± 0.026	7.5	0.3873	0.3855
${}_2S_3$	1.241	0.612 ± 0.082	14.0	0.6677	0.6681
${}_1S_2$	0.680	4.396 ± 0.285	6.5	4.1733	4.1859

f is the multiplet degenerate frequency as predicted for model 1066A. b is the Zeeman splitting parameter from equation (2), and r is the relative error in b. b_{1066A} and b_{PREM} are the predictions for the respective models based on Dahlen (1968).

Encoding of 3D Density Structure in Mode Spectra

The reduced symmetry of aspherical Earth models has as a direct consequence the removal of the degeneracy of the singlet eigenfrequencies: the multiplets are split. Within the framework of first-order perturbation theory this splitting can be linearly related to aspherical structure. Consider the kth multiplet, ${}_nS_\ell$. Its splitting can be described with the so-called aspherical structure coefficients, ${}_kc_s^t$. The structure coefficients are linearly related to aspherical structure of harmonic degree, s, and azimuthal order, t, through (Woodhouse and Dahlen, 1978)

$$ {}_kc_s^t = \int_0^a \left({}_kP_s \frac{\alpha_s^t}{\alpha_0} + {}_kS_s \frac{\beta_s^t}{\beta_0} + {}_kD_s \frac{\rho_s^t}{\rho_0} \right) dr, \qquad (3) $$

where $\alpha_s^t(r)$, $\beta_s^t(r)$, and $\rho_s^t(r)$ are the sought spherical harmonic expansion coefficients of V_p, V_s, and density, ρ, and quantities with a subscript zero refer to the spherically symmetric reference model. Furthermore, ${}_kP_s(r)$, ${}_kS_s(r)$, and

${}_kD_s(r)$ are the kernels relating the relative volumetric perturbations of harmonic degree s to the mode splitting as represented by the aspherical structure coefficients.

The kernels of the modes ${}_0S_{23}$ and ${}_{18}S_4$ are shown in Figure 9. While V_p, V_s, and density kernels are all of similar amplitude, they differ in one very important aspect: V_p and V_s kernels have (at least for one of the two modes) a positive mean value, while the density kernels oscillate for both modes around a zero mean. This situation is representative for all modes for which the structure coefficients, c_s^t, could be estimated. For the linear inverse problem posed in equation (3), this means that any density model with a nonzero mean for a particular spherical harmonic degree s and order t lies outside the space spanned by the set of kernels that belong to our structure coefficients. Hence our data do not allow us to make any inference on such models. To give an example: a model with a constant excess ellipticity in density of 1% $[\rho_2^0(r)/\rho_0(r) = -0.01]$ leads to no additional mode splitting and cannot by reconstructed from our structure coefficients. The only exceptions are the handful of modes below 1 mHz for which the density kernels do not integrate to zero (see Fig. 10).

For completeness we mention that inversions for 3D perturbations can also be carried out in the parameter space (μ, K, ρ). The sensitivity kernels in this representation are significantly different from the kernels in a (V_p, V_s, ρ) rep-

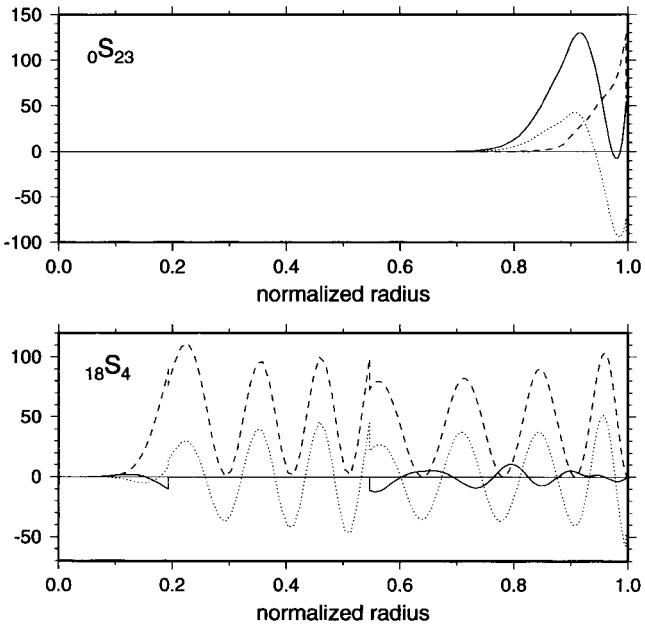

Figure 9. Sensitivity kernels for two modes with well-observed structure coefficients: the fundamental mode ${}_0S_{23}$ and the overtone ${}_{18}S_4$. The V_p kernels (dashed) and for ${}_0S_{23}$ also the V_s kernel (solid) have a positive mean value, while the density kernels (dotted) oscillate for both modes around a zero mean value. ${}_{18}S_4$ is a PKIKP-equivalent mode, and as such it is not expected to have much sensitivity to V_s structure.

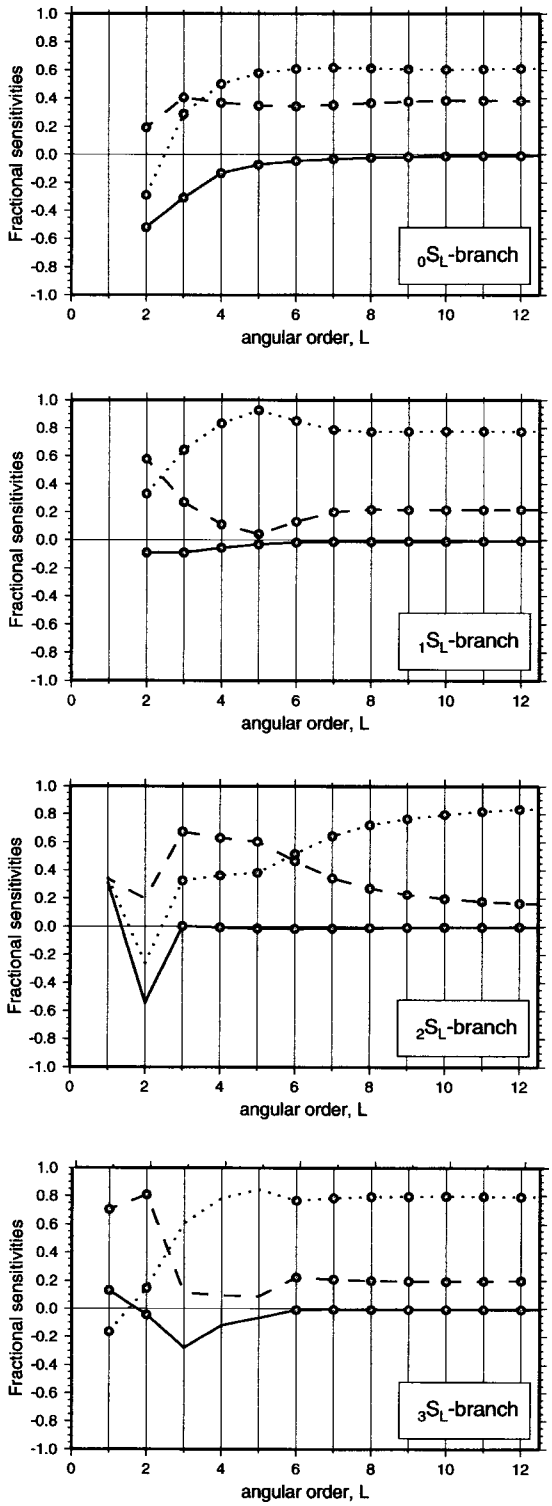

Figure 10. Relative sensitivity of aspherical structure coefficients to 3D perturbations of spherical harmonic degree $s = 2$ in V_p (dashed), V_s (dotted), and density (solid). Previously observed modes are indicated with a circular symbol. Note that density sensitivity is only significantly different from zero for modes below 1 mHz. (See also figure 22 in Ritzwoller and Lavely [1995].)

resentation (equation A6 in Ritzwoller and Lavely [1995]). However it turns out that in that representation μ and ρ are well-constrained model parameters, while incompressibility K is as ill constrained as ρ in the (V_p, V_s, ρ) representation (see fig. 31 in Ritzwoller and Lavely [1995]). In other words, independent of the chosen parameterization, we are largely unable to estimate three independent parameters. The only exception to this bleak situation is the splittings of modes below 1 mHz, which, through the effect of self-gravitation, posses additional sensitivity to density.

Whether 3D density structure can be estimated independently of V_p and V_s structure is hotly debated in the literature. On the one hand Ishii and Tromp (1999) claimed to succeed in the endeavor by adding geoid information, while Masters *et al.* (2000) presented a number of inversion experiments to show that no significant improvement in the fit to the observed structure coefficients can be achieved by allowing for 3D density structure. More recently Resovsky and Trampert (2002) presented supporting evidence for Ishii and Tromp (1999), while the findings of Kuo and Romanowicz (2002) corroborated the assessment of Masters *et al.* (2000).

The observation that density kernels in the (V_p, V_s, ρ) representation are essentially zero mean for modes above 1 mHz constitutes a strong argument in favor of the conclusions by Masters et al. (2000).

Conclusions

We have shown that below 1.5 mHz the most recent generation of SGs is competitive with the best spring gravimeters and seismometers. In addition SGs recording the recent, large Peruvian earthquake have produced spectra with some of the highest SNRs for the modes below 0.6 mHz since the beginning of digital seismometry. The band in which SGs excel is also the band where splitting of modes possesses comparatively high sensitivity to 3D density structure in the Earth's mantle and core. To observe this splitting and constrain lateral density structure is one avenue of research for which SGs are uniquely suited.

While the number of SGs will always be small (for reasons of price and complexity) compared to the number of sensors deployed in the GSN, the potential of a sparse network of gravimeters for normal-mode research has been demonstrated by the sparse IDA network (Agnew *et al.*, 1986), which was the workhorse for research in low-frequency seismology for 20 years.

Acknowledgments

I thank Walter Zürn for numerous discussions and critical inputs and Jacques Hinderer for the SG data from J9. The network centers of the German Regional Seismic Network and the IRIS/DMC for archiving and distributing the data from the different sensors at BFO are greatfully acknowledged. Constructive comments by David Crossley and an anonymous reviewer helped to improve this manuscript. All figures have been generated with GMT (Wessel and Smith, 1991).

References

Agnew, D., and J. Berger (1978). Vertical seismic noise at very low frequencies, *J. Geophys. Res.* **83,** 5420–5424.

Agnew, D., J. Berger, W. Farrell, F. Gilbert, G. Masters, and D. Miller (1986). Project IDA: a decade in review, *EOS* **67,** 203–212.

Astiz, L., and K. Creager (1995). Noise study for the federation of digital seismic stations, FDSN Station Book, www.fdsn.org/FDSNstation .htm (last accessed June 2003).

Backus, G., and F. Gilbert (1961). The rotational splitting of the free oscillations of the earth, *Proc. Natl. Acad. Sci.* **47,** 362–371.

Banka, D., and D. Crossley (1999). Noise levels of superconducting gravimeters at seismic frequencies, *Geophys. J. Int.* **139,** 87–97.

Crossley, D., J. Hinderer, G. Casula, H.-T. Hsu, Y. Imanshi, G. Jentzsch, J. Kaarianen, J. Merriam, Z. Meurers, J. Neumeyer, B. Richter, K. Shibuya, T. Sato, T. Van Dam (1999). Network of superconducting gravimeters benefit a number of disciplines, *EOS* **80,** 125–126.

Dahlen, F. (1968). The normal modes of a rotating, elliptical earth, *Geophys. J. R. Astr. Soc.* **16,** 329–367.

Dahlen, F. (1979). The spectra of unresolved split normal mode multiplets, *Geophys. J. R. Astr. Soc.* **58,** 1–33.

Dziewonski, A., and D. Anderson (1981). Preliminary Reference Earth Model (PREM), *PEPI* **25,** 297–356.

Ekström, G. (2001). Time domain analysis of the earth's background seismic radiation, *J. Geophys. Res.* **106,** 26,483–26,494.

Gilbert, F., and A. Dziewonski (1975). An application of normal mode theory to the retrieval of structural parameters and source mechanisms from seismic spectra, *Phil. Trans. R. Soc. Lond.* **A278,** 187–269.

Goodkind, J. M. (1999). The superconducting gravimeter, *Rev. Sci. Instrum.* **70,** 4131–4152.

Ishii, M., and J. Tromp (1999). Normal-mode and free air gravity constraints on lateral variations in velocity and density of the Earth's mantle, *Science* **285,** 1231–1236.

Kuo, C., and B. Romanowicz (2002). On the resolution of density anomalies in the earth's mantle using spectral fitting of normal mode data, *Geophys. J. Int.* **150,** 162–179.

Masters, T. G., and R. Widmer (1995). Free-oscillations: frequencies and attenuations, in *Global Earth Physics: A Handbook of Physical Constants*, T. J. Ahrens (Editor), American Geophysical Union, Washington, D.C., 104–125.

Masters, G., J. Park, and F. Gilbert (1983). Observations of coupled spheroidal and toroidal modes, *J. Geophys. Res.* **88,** 10,285–10,298.

Masters, G., G. Laske, and F. Gilbert (2000). Matrix autoregressive analysis of free-oscillation coupling and splitting, *Geophys. J. Int.* **143,** 478–489.

Nawa, K., N. Suda, Y. Fukao, T. Sato, Y. Tamura, K. Shibuya, H. McQueen, H. Virtanen, and J. Kääriäinen (2000). Incessant excitation of the earth's free oscillations: global comparison of superconducting gravimeter records, *Phys. Earth Planet. Interiors* **120,** 289–297.

Nishida, K., N. Kobayashi, and Y. Fukao (2000). Resonant oscillations between the solid earth and the atmosphere, *Science* **287,** 2244–2246.

Nishida, K., N. Kobayashi, and Y. Fukao (2002). Origin of Earth's ground noise from 2 to 20 mHz, *Geophys. Res. Lett.* **29,** 52-1–52-4.

Peterson, J. (1993). Observations and modeling of seismic background noise, *U.S. Geol. Surv. Open-file Rept. 93-322*, 1–45.

Press, W. H., B. P. Flannery, S. A. Teukolsky, and W. T. Vetterling (1987). *Numerical Recipes*, Cambridge U Press, New York.

Resovsky, J., and M. Ritzwoller (1998). New and refinded constraints on the three-dimensional earth structure from normal modes below 3 mHz, *J. Geophys. Res.* **103,** 783–810.

Resovsky, J., and J. Trampert (2002). Reliable mantle density error bars: an application of the neighbourhood algorithm to normal-mode and surface wave data, *Geophys. J. Int.* **150,** 665–672.

Richter, B., H.-G. Wenzel, W. Zürn, and F. Klopping (1995). From chandler wobble to free oscillations: comparison of cryogenic gravimeters and other instruments in a wide period range, *Phys. Earth Planet. Interiors* **91,** 131–148.

Ritzwoller, M., and E. Lavely (1995). Three-dimensional seismic models of the earth's mantle, *Rev. Geophys.* **33,** 1–66.

Ritzwoller, M., G. Masters, and F. Gilbert (1988). Constraining aspherical structure with low-frequency interaction coefficients: application to uncoupled multiplets, *J. Geophys. Res.* **93,** 6369–6396.

Romanowicz, B., M. Cara, J. F. Fels, and G. Roult (1984). GEOSCOPE: a French initiative in long period three component global seismic networks, *EOS* **65,** 753–756.

Smith, M., and G. Masters (1989). Aspherical structure constraints from free oscillation frequency and attenuation measurements, *J. Geophys. Res.* **94,** 1953–1976.

Suda, N., K. Nawa, and Y. Fukao (1998). Earth's background free oscillations, *Science* **279,** 2089–2091.

Van Camp, M. (1999). Measuring seismic normal modes with the GWR C021 superconducting gravimeter, *Phys. Earth Planet. Interiors* **116,** 81–92.

Warburton, R. J., and E. W. Brinton (1995). Recent developments in GWR instruments' superconducting gravimeters, in *Cahiers du Centre Européen de Géodynamique et de Séismologie, Proc. of the Second Workshop*, Nontidal gravity changes: intercomparison between absolute and superconducting gravimeters. Vol. 11, 23–56.

Warburton, R. J., and J. M. Goodkind (1977). The influence of barometric pressure variations on gravity, *Geophys. J. R. Astron. Soc.* **48,** 281–292.

Wessel, P., and H. F. Smith (1991). Free software helps map and display data, *EOS* **72,** 441.

Widmer, R., G. Masters, and F. Gilbert (1992a). Observably split multiplets: data analysis and interpretation in terms of large-scale aspherical structure, *Geophys. J. Int.* **111,** 559–576.

Widmer, R., W. Zürn, and G. Masters (1992b). Observation of low order toroidal modes from the 1989 Macquarie rise event, *Geophys. J. Int.* **111,** 226–236.

Widmer-Schnidrig, R. (2002). Application of regionalized multiplet stripping to retrieval of aspherical structure constraints, *Geophys. J. Int.* **148,** 201–213.

Woodhouse, J., and F. Dahlen (1978). The effect of a general aspherical perturbation on the free oscillations of the earth, *Geophys. J. R. Astron. Soc.* **53,** 335–354.

Zürn, W., and R. Widmer (1995). On noise reduction in vertical seismic records below 2 mHz using local barometric pressure, *Geophys. Res. Lett.* **22,** 3537–3540.

Zürn, W., G. Laske, R. Widmer-Schnidrig, and F. Gilbert (2000). Observation of Coriolis coupled modes below 1 mHz, *Geophys. J. Int.* **143,** 113–118.

Black Forest Observatory
Institute of Geophysics
Stuttgart University
Heubach 206
D-77709 Wolfach, Germany
widmer@geophys.uni-stuttgart.de
(R.W.-S.)

Manuscript received 2 July 2002.